Igneous Activity in the Bornu Basin, Onshore NE Nigeria; Implications for Opening of the South Atlantic

A. A. Suleiman[1], C. Magee[1], C. A.-L. Jackson[1], A. J. Fraser[1],

Affiliation:

[(1)]Basins Research Group (BRG), Department of Earth Sciences & Engineering, Imperial College, Prince Consort Road, London, SW7 2BP, UK

Corresponding author: c.magee@imperial.ac.uk

Abstract

The structure of igneous plumbing systems in circum-South Atlantic, intra-continental rift basins, e.g., the West and Central African Rift Systems (WCARS), remains enigmatic due to poor subsurface data coverage and quality. How magmatism in these basins related to the opening of the South Atlantic is thus poorly understood. We integrate 2D and 3D seismic reflection data (c. 27600 km^2), data from 23 boreholes, and field observations from the Bornu Basin and Upper Benue Trough, onshore NE Nigeria to examine the timing and development of igneous bodies possibly related to opening of the South Atlantic. We identify numerous sills, which typically have saucer-shaped and en-echelon morphologies, and extrusive volcanic cones. The igneous rocks are alkali basalts and dolerites. Seismic-stratigraphic relationships indicate that emplacement occurred in the Early Cretaceous (Albian-to-Cenomanian; ca. 120 Ma), Late Cretaceous (Santonian-to-early Campanian; ca. 83 Ma), and Cenozoic (Miocene; ca. 22 Ma). Magmatism was broadly coeval with major plate boundary interactions, characterized by major azimuthal changes in fracture zones in the developing South

Atlantic Ocean. The broad temporal correlation between intra-continental rift basin magmatism and plate boundary interactions suggests that periods of magma emplacement may have, in some way, been instigated by stress dissipation into intra-continental rift basins.

Introduction

The break-up of Gondwana and subsequent opening of the South Atlantic by rifting of the African and South American plates was associated with crustal extension, compression, and strike-slip tectonics in both passive margin and intra-plate rift systems (e.g., Fairhead, 1988; Benkhelil, 1989; Guiraud and Maurin, 1992; Davison, 1997; Pérez-Díaz and Eagles, 2014). Intra-continental deformation was accommodated by the development of normal fault arrays and post-rift tectonic inversion. In some cases, intra-continental deformation was also associated with melt generation and magma emplacement, suggesting that igneous activity may relate to and thus provide critical insight into the timing and evolution of plate geodynamic episodes (Sengör and Burke, 1978; Benkhelil, 1989; White and McKenzie, 1989). However, a key barrier to understanding the link between plate margin and intra-plate tectono-magmatic processes is the paucity of age constraints on the timing of igneous activity. Where intra-continental rift basins containing magmatic rocks occur on the African margin of the South Atlantic, the lack of relative timing constraints principally reflects a paucity of outcrops from which to collect igneous rock samples. Furthermore, the typical availability of only sparse, low-quality subsurface data means that it is difficult to accurately establish the structure and age of Gondwana breakup-related rift basins.

Numerous tectono-magmatic studies have demonstrated that seismic data and field observations can be used to decode the geometry, distribution, and timing of magmatism in sedimentary basins worldwide, thereby allowing contemporaneous tectonic processes to be established (e.g., Skogseid et al., 1992; Symonds et al., 1998; Planke et al., 2000; Smallwood and Maresh, 2002; Planke et al., 2005; Hansen and Cartwright, 2006a; Jackson et al., 2013; Schofield et al., 2015). In particular, seismic reflection data permit direct imaging of igneous bodies and basin structure, with borehole data and seismic-stratigraphic observations allowing the timing of igneous activity to be constrained (e.g., Smallwood and Maresh, 2002; Trude et al., 2003; Magee et al., 2013c). Here, we use newly available seismic reflection, borehole, biostratigraphic, and petrological data from the Bornu Basin and Upper Benue Trough, onshore NE Nigeria to constrain the regional tectono-magmatic history of this portion of the West and Central African Rift Systems (WCARS) (Fig. 1). We document the geometry and distribution of igneous intrusions and extrusions in the basin and determine the mechanics of magma emplacement. We show that a range of processes, from brittle failure to non-brittle deformation (fluidization) of the host rock, facilitated magma emplacement and controlled the final geometry of intrusions in the Bornu Basin (e.g., Polteau et al., 2008; Jackson et al., 2013; Magee et al., 2013c). For the first time in the Bornu Basin and the WCARS, we apply the concept of seismic-stratigraphy and use biostratigraphic dating to constrain the timing of the three, discrete igneous events in the Early Cretaceous (Albian-to-Cenomanian; ca. 120 Ma), Late Cretaceous (Santonian-to-early Campanian; ca. 83 Ma), and Cenozoic (Miocene; ca. 22 Ma). These age constraints enable us to investigate how intra-continental magmatism is temporally related to regional tectonic events associated with the breakup of Gondwana and opening of South Atlantic Ocean.

Geological setting

The Bornu Basin is an intra-continental, Cretaceous-to-Holocene rift basin located in NE Nigeria (Fig. 1) (Avbovbo et al., 1986). Numerous studies suggest that basin formation involved Early Cretaceous extension, Late Cretaceous shortening, and a period of relative tectonic quiescence in the Cenozoic (Figs 2 and 3) (Avbovbo et al., 1986; Genik, 1992; Fairhead et al., 2013). The oldest rocks in the Bornu Basin consist of Precambrian-to-Lower Paleozoic migmatites and granite, with the oldest sedimentary strata corresponding to the Lower Cretaceous (Albian-to-Cenomanian) lacustrine and terrestrial deposits of the Bima Sandstone (Fig. 2) (Carter et al., 1963; Avbovbo et al., 1986; Guiraud, 1990; Samaila et al., 2006). The Bima Sandstone is overlain by estuarine-to-marine deposits of the Gongila Formation (Cenomanian-to-Turonian), which is itself overlain by the Fika Shale, a marine unit deposited during a major transgression in the Turonian-to-Campanian (Fig. 2) (Carter et al., 1963). Estuarine-to-deltaic clastics of the Gombe Sandstone (Maastrichtian), which is best-developed in the Upper Benue Trough, overlie the Fika Shale (Fig. 2) (Carter et al., 1963). The non-marine Kerri-Kerri Formation (Paleogene) was unconformably deposited onto the Gombe Sandstone in the Upper Benue Trough and the Fika Shale across most of the Bornu Basin; the boundary between these units marks the regional Cenozoic unconformity (Fig. 2) (Carter et al., 1963; Genik, 1992; Obaje et al., 2004a; Obaje et al., 2004b). The youngest rocks in the basin belong to the Quaternary Chad Formation, which largely consist of lacustrine and alluvial sedimentary strata (Fig. 2) (Carter et al., 1963).

The structure of the Bornu Basin is defined by an array of basement-involved, NE-SW-striking normal faults that bound a series of horst and graben (e.g., Figs 3 and 4a). These faults are c. 70 km long and dip towards the NW, extending upward into and tipping out within Cretaceous strata (e.g., Fig. 3) (Avbovbo et al., 1986). Basement-detached, strata-bound faults are also developed in the Bornu Basin, being largely confined to the Cretaceous interval and having their upper tips truncated along the regional Cenozoic unconformity. These strata-bound faults strike predominantly NE-SW, although some strike NW-SE. Spatially related to these two fault populations are a series of asymmetric, low-amplitude antiforms and synforms, which have axial planes striking broadly parallel to the basin-bounding faults (Figs 3 and 4a) (Avbovbo et al., 1986). Studies of the neighbouring Doseo and Muglad basins suggest that these folds formed due to Santonian (ca. 83 Ma) inversion tectonics and strike-slip faulting, the latter being expressed in the form of flower structures (Genik, 1992).

A number of studies have identified evidence for Cretaceous igneous activity in the Bornu Basin and neighbouring Benue Trough (Avbovbo et al., 1986; Benkhelil et al., 1988; Benkhelil, 1989; Genik, 1992; Alalade and Tyson, 2013). For example, seismic reflection and gravity data presented by Avbovbo et al., (1986) indicate that a series of NW-trending intrusive igneous bodies occur at relatively shallow depths in the Bornu Basin, although the detailed geometry and distribution of these remained poorly constrained due to the poor imaging of the 2D seismic data. In the Upper Benue Trough, two distinct phases of magmatic activity have been identified based on field studies: (i) activity associated with the emplacement of the Mesozoic Burashika Complex (Fig. 1); and (ii) activity associated with the Cenozoic (22-11 Ma) Cameroon Volcanic Line (Carter et al., 1963; Grant et al., 1972b). Extrusive volcanic breccias, tuffs and intrusions are also identified in the Lower Benue Trough in the Asu River Group

(Albian) (Benkhelil, 1989). The geometry, distribution and exact timing of emplacement of these igneous bodies, and how the associated magmatic activity may relate to regional tectonic events, remain poorly understood.

Dataset and Methodology

We use 2D and 3D seismic reflection surveys covering a total area of c. 27,600 km^2 (Fig. 1). The 2D seismic dataset has an irregular line spacing of c. 0.5 to 20 km, with line lengths ranging from c. 13-92 km (Fig. 1). 2D seismic data image down to 6 seconds TWT. The vertical resolution of the 2D seismic data within the broad interval of interest is c. 30 m, based on a dominant frequency of 22 Hz (±10%) and a Fika Shale interval velocity of 2414 m/s (±10%) (obtained from the Bulte well; Fig. 4b). The 2D seismic data are minimum phase, with red reflections (peaks) representing a downward increase in acoustic impedance and blue reflection (trough), representing a downward decrease in acoustic impedance. The 3D seismic data are also minimum phase, having a bin spacing of 25 m by 25 m. In the 3D volume, a dominant frequency of 34 Hz (±10%) in the interval of interest and a Fika Shale interval velocity of 2414 m/s (±10%) yield an approximate vertical resolution of c. 20 m.

Twenty three wells are available in the study area (Fig. 1), with most containing thin sections of well cuttings, and a suite of logs (e.g. sonic (DT), gamma ray (GR), and density (RHOB); some contain resistivity logs. The wells are used to constrain basin-fill composition, the age of the deformed and intruded successions, and the composition of the intrusions. Field observations in the neighbouring Upper Benue Trough are used to constrain the sub-seismic geometry of igneous bodies, and aspects of host rock composition and magma-host rock interactions imaged in the Bornu Basin.

A range of seismic attributes, including reflection intensity, relative acoustic impedance and instantaneous frequency, were used to locate and map 53 igneous bodies, of which 26 occur within the 3D seismic volume (Figs 4b and c). The seismic expression of igneous intrusions is non-unique (Smallwood and Maresh, 2002; Magee et al., 2015). For example, sandstone intrusions (Dixon et al., 1995; Huuse and Mickelson, 2004), high acoustic impedance sedimentary rocks such as coals (Xu et al., 2009; Xu et al., 2010), and diagenetic boundaries such as the opal-ACT transition (Berndt et al., 2004; Zampetti et al., 2005) can all be expressed as high-amplitude reflection anomalies. Thus, we used the following criteria to identify igneous reflections in the seismic data: (i) borehole data that tie high-amplitude reflections to igneous rocks; (ii) high-amplitude reflections cross-cutting sedimentary strata; (iii) high-amplitude reflections that are laterally discontinuous; and (iii) similarities in size and geometry to igneous intrusions described in previous studies (e.g., Hansen and Cartwright, 2006; Magee et al. 2015; Planke et al., 2015).

The estimated vertical resolution of the seismic data (c. 30 m in the 2D data and c. 20 m in the 3D data) allow us to constrain the minimum thickness of the igneous bodies imaged in the seismic reflection data. Sills thinner than the estimated vertical resolution are expressed as tuned reflection packages, from which the lower and upper intrusive contacts cannot be separately resolved (Smallwood and Maresh, 2002; Magee et al., 2015). Magma flow indicators such as intrusive steps, bridge structures and magma lobes are observed in the mapped sills (Fig. 5) (Schofield et al., 2012a; Schofield et al., 2012b; Magee et al., 2013c; Magee et al., 2014; Schofield et al., 2015). These magma flow indicators also provide important insights into sill emplacement mechanics; e.g., intrusive steps form in response to brittle fracture propagation, typically at burial depths ≥2 km (Pollard et al., 1975; Schofield et al., 2012b), whereas magma fingers form through non-brittle emplacement, commonly in response to host rock fluidization at burial depths ≤2 km (Pollard et al., 1975; Rickwood, 1990; Schofield et al., 2010; Schofield et al., 2012a; Schofield et al., 2012b).

Results

Basin structural style

A depth-structure map of the base of the Bima Sandstone indicates that the study area can be divided into two sub-basins; the eastern (ESB) and western (WSB) sub-basins (Fig. 4a). Faults within and bounding the WSB typically dip at 40˚-60˚ and strike NE-SW, whilst those in the eastern sub-basin dip at 40˚-55˚ and strike NW-SE (Fig. 4a). Isolated half-graben within the ESB are, however, bound by faults that strike NE-SW. Some of the normal faults, especially those striking NE-SW, display evidence for minor inversion in the form of low-amplitude hanging wall folds, whereas those striking NW-SE are associated with flower structures (Figs 3 and 4a).

Basin stratigraphy

To provide context for the description of the igneous bodies, here we describe the architecture of the main sedimentary packages in the study area and relate their deposition to the tectonic evolution of the basin. The Bima Sandstone thickens across the main basin-bounding faults and is accordingly interpreted as being a syn-rift sequence deposited during the main phase of Early Cretaceous rifting (Fig. 3). The Gongila Formation overlies the Bima Sandstone and its seismic architecture shows better reflection continuity and parallelism (Fig. 3); the Gongila Formation is interpreted to be post-rift sequence as it does not thicken across faults and is largely unfaulted, capping faulted Bima Sandstone (Fig. 3). The Fika Shale conformably overlies the Gongila Formation thinning across and onlapping onto the fault-parallel anticlines developed in the immediate hanging walls of the basin-bounding faults (Fig. 3). Based on this seismic-stratigraphic architecture, we interpret that the Fika Shale forms part of the post-rift 'syn-inversion' sequence. The Kerri-Kerri Formation unconformably overlies Fika Shale and its seismic architecture is sub-parallel (Fig. 3). We interpret that the Kerri-Kerri Formation was deposited after the main phase of inversion during a period dominated by simple subsidence, probably driven by post-rift cooling of the crust. Likewise, we interpret that the overlying, broadly tabular Chad Formation is part of the post-inversion sequence (Fig. 3). Well correlations show that these major stratigraphic units contain range of lithological units such as shale, sandstone and claystone (Fig. 6).

Igneous bodies

The occurrence of igneous rocks within the Bornu Basin is confirmed by the recovery of dolerite cuttings from four wells in the study area; these dolerites are primarily composed of plagioclase, clinopyroxene (augite), and Fe-Ti oxides. The thickest sill intersected by a well is c. 150 m thick (Albarka well; Fig. 4b). Igneous bodies are expressed in wireline-logs (Nelson et al., 2009) by low (c. 29 API) gamma ray and high (c. 177 m/ms) sonic values (Fig. 6).

The mapped intrusions typically appear as strata-discordant or concordant, laterally discontinuous (maximum length of c. 14 km in this study), high-amplitude anomalies (e.g., Fig. 2). Igneous intrusions are imaged in seismic data and primarily occur in the Cretaceous units, particularly the Fika Shale marine shales, the fluvial Bima Sandstone, and the heterolithic, coastal plain to estuarine deposits of the Gongila Formation (Figs 2 and 6). Most intrusions occur below the regionally developed Cenozoic unconformity but, on very rare occasions, some intrusions appear to cross-cut the unconformity and extend upward into the continental sandstone of the Kerri-Kerri Formation by ~75 ms (Fig. 7). We identify three major geometrical styles of igneous bodies within our seismic data: (i) Type-1 saucer-shaped sills; (ii) Type-2 strata-concordant sills; and (iii) Type-3 volcanic cones.

Type-1: these are saucer-shaped, high-amplitude reflections consisting of a strata-concordant base that passes laterally into a transgressive, inwardly dipping, inclined limb. They are the most common type of intrusion mapped in the study area being developed in the ESB and WSB. They occur across a wide depth range; spanning 500-2000 m. Here, we describe the detailed morphology of one representative saucer-shaped sill (Sill-1, Fig. 8).

Sill-1 was emplaced into the Fika Shale (Fig. 8). It covers an area of c. 6 km^2, has a strata-concordant inner sill that is up to c. 2500 m in diameter, is c. 40-55 m thick, and contains a series of positive ridges on its surface that demarcate steps in the seismic reflection (Fig. 8a). Intrusive step long axes radiate outward from the deepest, central point of the sill. A planar inclined sheet, which transgresses up to c. 200 m of stratigraphy, occurs around the margins inner sill (Fig. 8a and b). The map-view of the Sill-1 illustrates that the sill can be sub-divided into semi-circular lobes that are superimposed onto the overall geometry (Fig. 8a). The inclined limb of the Sill-1 appears to terminate against a flower structure, the steeply dipping boundary faults of which encompass the entire circular intrusion (Fig. 8c). A fold that directly overlies the sill is observed, which has a box-like geometry with a flat top and steep limbs that terminate against flower structure faults (Fig. 8c). Strata above and beneath the sill are displaced upwards by c. 100 ms relative to corresponding reflections in the footwall of the flower structure (Fig. 8c).

Type-2: these sills are expressed as en-echelon geometry, high amplitude reflections (e.g., Figs 9 and 10). They are developed in both the ESB and WSB and occur across a wide depth range (500-2000 m). Type-2 sills are characterized by transgressive internal limbs. Here, we describe the detailed morphology of two representative sills (Sill-2, Fig. 9; Sill-3, Fig. 10).

Sill-2 is asymmetric and has a diameter of c. 4000 m (Fig. 9a). It covers c. 11 km^2 and is c. 65 m thick at its centre, reducing in thickness to c. 30 m at the en-echelon transgressive limb or branching sheet (Fig. 9). Sill-2 is gently dipping and is thus weakly disconcordant with the encasing Fika Shale host-rock (Figs 9b and c). Sill-2 becomes more strata-discordant towards its distal end, where it turns into an inclined sheet that has a relief of c. 220 m (Figs 9a-c). No intrusion-related deformation, such as host rock forced folding or substantial faulting is observed in association with Sill-2 (Figs 9b-d). Sill-2 comprises a linked network of sill lobes that merge together to form a single body (Fig. 9a). The point of coalescence between adjacent lobes is marked by a series of intrusive steps and broken-bridges, which appear to radiate out from the deepest central point of the sill (Figs 9a and d).

Sill-3 is at least c. 14000 m in length although, due to being imaged in 2D data only, its full areal extent cannot be constrained (Fig. 10). Sill-3 is c. 85 m thick at its centre, reducing in thickness to c. 40 m at the en-echelon inclined limb (Fig. 10). Sill-3 is more strata-discordant towards its distal end, where it turns into an inclined sheet that has a relief of c. 360 m (Fig. 10). It is important to highlight that the inclined sheet here appears planar and non-transgressive, unlike the one observed in Sill-2 (Figs 9 and 10).

Furthermore, an overlying open antiform, with amplitude of c. 760 m, overlies Sill-3; the lateral terminations of the fold directly overlie the seismically resolved lateral sill tips (Fig. 10). Overlying Upper Fika Shale on-laps on the fold and both the Fika Shale and Gongila Formation are truncated at their tops by the regional Cenozoic unconformity (Fig. 10).

Type-3: A single high-amplitude, mound-like feature (i.e. Type-3) is observed on top of the Bima Formation in the WSB (Fig. 11a). This broadly conical structure is c. 3000 m in diameter and has a height of c. 380 m (Fig. 11a). Intra-mound reflections downlap the underlying Bima Sandstone and are sub-parallel to mound upper surface (Fig. 11a).

Similar conical structures resting upon the Bima Sandstone, which are up to c. 400 m tall and c. 1000 m in diameter, are observed in the field in the neighbouring Upper Benue Trough (e.g., Fig. 11b). Xenoliths of the Bima Sandstone were observed in some of the rocks that comprise the volcanic cones (Fig. 11c). Petrological analyses reveal that these conical structures are composed of fine-grained (<0.5 mm groundmass), porphyritic alkali basaltic rocks that primarily consist of olivine (up to c. 25%), clinopyroxene (up to c. 20%), and plagioclase (up to c. 40%) (e.g., Fig. 11d). Glass is present in some of the samples collected and minor alkali feldspar (c. <10%), nepheline (c. <8%), and Fe-Ti oxides (c. <10%) are also observed. Plagioclase only occurs in the groundmass and forms elongated laths that occasionally display a trachytic texture (e.g., Fig. 11d). Phenocrysts are dominated by olivine and clinopyroxene, both of which are up to 4 mm in diamater and typically display euhedral to subhedral habits (e.g., Fig. 11d).

Interpretation

Emplacement mechanics and depth of intrusion

Type-1: these reflections correspond to saucer-shaped sills (Fig. 8) (Malthe-Sørenssen et al., 2004; Thomson and Hutton, 2004; Hansen and Cartwright, 2006a, b; Polteau et al., 2008; Jackson et al., 2013). The radial disposition of steps, interpreted as intrusive steps, away from the deepest point of the inner sill (e.g. Sill-1, Figs 8a and b) suggest that this intrusion formed through the coalescence of at least five magma segments that propagated radially away from the inner sill centre (Schofield et al., 2012b; Magee et al., 2013c). The overall saucer-shaped geometry of the Type-1 sills implies that they formed at relatively shallow-levels (Malthe-Sørenssen et al., 2004; Hansen and Cartwright, 2006a; Magee et al., 2013a). However, the occurrence of intrusive steps, which are typically associated with brittle emplacement at deeper burial depths, suggests that either the depth of emplacement was not too shallow as to inhibit fracturing and/or that the host rock rheology allowed brittle deformation (Schofield et al., 2012b).

The fold above Sill-1 (Fig. 8c) may have formed either: (i) synchronous to magma emplacement as an intrusion-induced forced fold, with the small faults directly above the sill possibly representing outer-arc stretching-related faults (Hansen and Cartwright, 2006b; Jackson et al., 2013; Magee et al., 2013a); or (ii) in response to strike-slip faulting before magma emplacement. We dismiss the former interpretation for the principal reason that strata beneath the sill are offset across the strike-slip faults by approximately the same amount as strata above the sill, suggesting that they were deformed in the same strike-slip faulting episode (Fig. 8c). This interpretation implies that the faulting and flower structure-related uplift occurred before the emplacement of Sill-1.

Type-2: we interpret these intrusive bodies as en-echelon transgressive sills (Figs 9 and 10). In a similar manner to the Type-1 sills, the radial disposition of the magma flow indicators away from the deepest centre of Sill-2 suggests magma emplacement from a point source (Fig. 9a). The superimposed sheets, each with an en-echelon structure, (Figs 9b, c, and 10) possibly indicate multiple intrusions of magma sheet formed in one of three ways (Fig. 12): (i) break-out of magma at the base of a pre-existing inclined sheet instigates sill propagation; (ii) inclined sheet development at progressively more proximal locations to the magma source, breaking out at the top of existing sheets due to the waning of magma pressure; or (iii) the emplacement of under-or over-accreted sills, resulting in the formation of a sill with different lateral dimensions and thereby different points of sill-inclined sheet transitions. The Type-2 sills are, therefore, composed of multiple, now merged sheets, which we interpret as magma lobes (e.g., Fig 9a). We interpret that the network of lobes within Sill-2 likely formed as the result of multiple magma segments intruded along bedding planes at shallow depth, which subsequently inflated vertically and laterally (Polteau et al., 2008; Galerne et al., 2011; Schofield et al., 2012a). We infer that the separation of the merged network of lobes at their distal ends and overall lateral thinning of the sills are related to a decrease in the volume of the magma supply which starved the merging lobes as they propagated (Vigneresse and Clemens, 2000; Magee et al., 2013c).

The presence of intrusive steps in the inner sill and inclined sheets suggest a typical brittle magma emplacement mechanism (Fig. 9) (Schofield et al., 2012b). The formation of intrusion-related fractures may be influenced by the presence of pre-existing fault and fracture systems in the host rock. This may explain the irregular and selective formation of the en-echelon transgressive limbs, with limbs preferentially forming in intervals where favourably orientated pre-existing faults occur (Magee et al., 2013c). This interpretation is supported by our observation that transgressive limbs are spatially related to faults. In some instances, however, inclined sheets do not appear to exploit pre-existing faults, but rather coincide with steeply oriented rock-rock interfaces. This is best-demonstrated in the inclined sheet that cross-cuts the Cenozoic unconformity, which could have propagated along compliant, sub-vertically orientated bedding in the Cretaceous succession (Fig. 7).

We interpret that Sill-3 was emplaced at palaeo-depth of c. 500 m. This is based on the presence of a supra-sill dome above the sill, interpreted as a forced fold that formed to accommodate magma emplacement, onto which overlying strata of the marine Fika Shale onlap (Fig. 10); i.e. the top of the fold represented the palaeo-surface during intrusion (e.g., Hansen and Cartwright, 2006b; Jackson et al., 2013). The age of the forced fold and, therefore, the timing of sill emplacement can also be constrained to the Santonian-to-early Campanian (ca. 83 Ma) by dating the supra-sill strata that onlap the fold (Trude et al. 2003; Jackson et al., 2013; Magee et al., 2013a; Magee et al. 2014). The precise 3D geometrical and spatial relationship between the sill and fold cannot be constrained using 2D seismic data alone. However, the following observations support our forced fold interpretation (Fig. 10): (i) the broad spatial correspondence between the intrusion and the fold; (ii) thinning of the supra-sill stratigraphy (i.e. Fika Shale) across the fold and; (iii) lack of volcanogenic seismic facies in the fold core, suggesting the structure has a non-volcanic origin (Hansen and Cartwright, 2006b; Thomson, 2007; Cukur et al., 2010; Jackson et al., 2013).

Type-3: we interpret that the high-amplitude cone-shaped structure observed in the WSB as a volcano because it has a similar geometry to the alkali basalt volcanic cones observed in the Upper Benue Trough (Fig. 11). The intra-cone reflections may represent the boundaries between individual lavas, or the boundaries between lavas and pyroclastic deposits (Fig. 11a) (Magee et al., 2013b). We interpret that the volcano was emplaced during the late Albian to Cenomanian, based on the observation that it sits directly on the Bima Sandstone; a similar age relationship is observed in the field in the neighbouring Upper Benue Trough where the alkali basalts also contain xenoliths of Bima Sandstone (Fig. 11c). The interpreted volcano could also be a hydrothermal vent (e.g., Planke et al., 2005).

Timing of igneous activity

Based on the age of strata hosting the intrusions, the age of emplacement of the igneous extrusions, and seismic-stratigraphic relationships in overlying strata, we interpret that three phases of igneous activity occurred in the Bornu Basin. The first phase likely occurred in the Early Cretaceous, based on the late Albian to Cenomanian age of the volcanic cone (Figs 11 and 13). Based on our observations that the Santonian-to-early Campanian Upper Fika Shale onlaps onto and thins across the intrusion related forced folds, we interpreted that the second phase of magmatic activity occurred in the Late Cretaceous (Fig. 10 and 13). It should be noted that, we cannot constrain the ages of some intrusions because of the lack of forced folding above them, however, these intrusions are obviously younger than the host rock (Santonian-to-early Campanian). We infer that the sills appearing to post-date strike-slip faulting belong to the Late Cretaceous phase of igneous activity (e.g., Sill-1, Fig. 9). Field studies in the Lower to Middle Benue Trough have reported volcaniclastic sedimentary rocks and other sub-volcanic intrusions in the Ogoja to Abakaliki area (Benkhelil, 1989). Chemical analysis of these samples reveals microgabbro, dolerite and alkaline syenites compositions, with

K-Ar dating suggesting ages of 104-70 Ma (i.e. Early to Late Cretaceous), which is broadly consistent with our inferences from seismic reflection data (Benkhelil, 1989).

Based on the truncation of Cenozoic regional unconformity by a solitary intrusion which is c. 1 km from the surface, we suggest that a third, Cenozoic phase of igneous activity may have occurred in the Bornu Basin (Figs 7 and 13). This inferred period of igneous activity, although based on very limited seismic-stratigraphic evidence, is consistent with radiometric ages reported from Cenozoic, principally Miocene (ca. 22-11 Ma) intrusives documented in the neighbouring Upper Benue Trough (Fig. 13) (Grant et al., 1972b).

Implications for opening of the South Atlantic Ocean

The integration of subsurface data from the Bornu Basin sub-surface datasets with outcrop observations from the neighbouring Upper Benue Trough provide insights into the geometry, distribution and age of emplacement of igneous bodies in the WCARS. Because we have established the relative age of igneous activity, we can thus investigate how this activity might relate to the plate boundary geodynamics occurring during opening of the South Atlantic (Fig. 13).

The earliest phase of igneous activity we identify occurred during the Early Cretaceous, broadly correlating with initial separation of the South American and African plates in the Albian (ca. 100 Ma) (Fig. 13). This phase of activity also coincided with a period of major igneous activity identified in other circum-South Atlantic rift basins, such as the neighbouring Benue Trough in the African plate, and the Campos, St. Helena and Rio Grande Rise areas of the South Atlantic plate (Fig. 13) (Torsvik et al., 2009). There is no change in the azimuth of the Kane Fracture Zone associated with this phase of igneous activity (Fig. 13).

During the Santonian-to-early Campanian, the main phase of igneous activity occurred in the Bornu Basin, during which most of the saucer-shaped sills and en-echelon sills were emplaced. Similar magmatic events are documented in the Benue Trough and in several southern Brazilian basins in the form of onshore and offshore alkaline-to-peralkaline magmatism (Fig. 13) (Torsvik et al., 2009). This second phase of igneous activity broadly correlates with the time when Gondwana was completely ruptured and oceanic crust was emplaced (ca. 83.5 Ma) (Fig. 13). Collision of the African and the Eurasian plates resulted in a change of stress regime in the South Atlantic Ocean and surrounding plates; this is preserved by a major change in the azimuth of the Kane Fracture Zone (Fig. 13) (Guiraud and Bosworth, 1997; Fairhead et al., 2013). This particular change in the intra-plate stress regime manifested as intra-plate shortening and tectonic inversion in the Bornu Basin, and the development of regional unconformities in several intra-continental rift basins such as Muglad and Doba basins (Fig. 13) (Fairhead, 1988; Genik, 1992; Guiraud and Bosworth, 1997; Fairhead et al., 2013).

The third and final phase of igneous activity, which occurred in the Cenozoic, appears to be coincident with a major phase of oceanic magmatism and another change in the azimuth of the Kane Fracture Zone (Fig. 13). This phase of activity broadly coincides with major intra-continental volcanism, such as that which occurred along the Cameron Volcanic Line (Fig. 13). The oldest of these Cenozoic igneous rocks are the Early Miocene (ca. 22 Ma) volcanics preserved in the Benue Trough (Grant et al., 1972b).

Factors such as mantle geodynamics (e.g., convection and mantle plumes), changes in the lithospheric thickness, and plate boundary interactions can result in intra-plate magmatism (e.g., Meeuws et al., 2016). Valentine and Perry (2007) argued that regions of basaltic volcanism can be divided into those that are magmatically and tectonically controlled; melt within magma-driven basaltic fields tends to be generated in response to thermal perturbations in the mantle, independent of tectonic processes, whereas tectonically controlled fields rely on and are therefore temporally associated with plate deformation facilitating magma accumulation and ascent. Our findings broadly suggest that the observed intra-plate magmatism along the aborted rifts of the African and possibly South American continents is genetically related to plate boundary geodynamics associated with the opening of the South Atlantic Ocean.

Conclusion

The methodologies employed in our study show how the investigation of magma emplacement mechanics and the 3D geometry of igneous bodies mapped in high resolution seismic reflection data can be used to constrain the timing and tectonic implication of intra-plate magmatism. We particularly examined igneous bodies in the Bornu Basin and Upper Benue Trough, onshore NE Nigeria using seismic reflection, borehole, field, and petrological data. The major igneous geometries identified in this study are: (i) saucer-shaped sills; (ii) strata-concordant sills; and (iii) volcanic cones. These bodies are alkali basalts or dolerites. Seismic-stratigraphic analysis of the igneous bodies and the related host rock deformation suggest emplacement occurred in the Early Cretaceous (Albian-to-Cenomanian; ca. 120 Ma), Late Cretaceous (Santonian-to-early Campanian; ca. 83 Ma), and Cenozoic (Miocene; ca. 22 Ma). The timing of magmatism identified in the study area is consistent with the timing of major plate boundary interactions, some of which are characterized by changes in the azimuth of the oceanic fracture zones. This suggests that periods of melt generation and emplacement in intra-continental rift basins may have recorded plate boundary geodynamics during opening of the South Atlantic Ocean.

Acknowledgement

We would like to acknowledgement the funding of this study by the Petroleum Technology Development Fund (PTDF), Nigeria. We are also grateful to the Nigerian National Petroleum Corporation (NNPC) for the datasets provision. Schlumberger are thanked for the software and our editors for the provision of a useful feedback. We are grateful to Peter Reynolds and an anonymous reviewer for their constructive comments and to Peter Clift for his editorial handling and revision suggestions.

Figure captions

Figure 1. Location of the seismic and borehole datasets used in this study from Bornu Basin and the field area studied in the Upper Benue Trough, onshore NE Nigeria.

Figure 2. Tectono-stratigraphic chart of the Bornu Basin and interpreted seismic section detailing the seismic-stratigraphy the major stratal units. Within the seismic data, the Gombe Formation is rarely observed due to erosion and formation of the Cenozoic unconformity.

Figure 3. a) Time-structure map of base Bima Sandstone showing the main fault patterns and styles. **b)** Distribution of igneous bodies at different depth levels in both the WSB and ESB. Note the absence of intrusion at the rift shoulders. **c)** 3D

geometries of intrusions, mapped across 3D seismic and closely spaced 2D seismic datasets in the ESB. See the Figure 4b for location.

Figure 4. Western Sub-basin structural style and major stratigraphic units in the Bornu Basin. The exact locations of fault planes are difficult to constrain, however, the presence of the folded hanging walls suggest reverse reactivation of the extensional normal faults. See Figure 4b for the line location.

Figure 5. a) Schematic diagram of a sill containing intrusive steps and bridge structures. **b)** Cross-sectional view of intrusive steps and a broken-bridge. **c)** Idealized sketch of magma finger and lobe components within a saucer-shaped sill. Step, bridge, finger, and lobe long axes all demarcate magma flow axes. Modified from Magee et al., (2016).

Figure 6. Lithological correlation across some six wells within the study area.

Figure 7. Seismic profile showing Cretaceous and lowermost Cenozoic successions, separated by the Cenozoic unconformity, cross-cut by an inclined, high-amplitude reflection. See Figure 4b for location.

Figure 8. a) Time-structure map of Sill-1 illustrating inferred magma flow directions. Contour spacing is 12 ms TWT. See Figure 3c for location. **b)** Arbitrary seismic profile highlighting the discordant nature of Sill-1, which displays intrusive steps. See Figure 8a for location. **c)** Sill-1 and a supra-sill fold bounded by strike-slip faults.

Figure 9. a) Time-structure map of Sill-2, which consists of merged lobes bounded by magma flow indicators. See Figure 3c for location. **b)** Branching sill limb that describe an en-echelon morphology. **c)** Transition between the concordant inner sill

and transgressive inclined limbs. **d)** Composite profile illustrating bridge and intrusive step structures. See Figure 9a for seismic line location.

Figure 10. Uninterpreted seismic section and line drawing showing the en-echelon nature of Sill-3 and the geometry of the overlying forced fold, onto which the Fika Shale onlaps.

Figure 11. a) Inferred volcanic cone, resting upon the Bima Sandstone, with gently sloping limbs and internal reflections that mirror the external geometry. **b)** Field photograph of a volcanic mound, composed of alkali basalt, on top of the Bima Sandstone within the Upper Benue Trough (Lat. 9°53'17.90"N, Long. 11°10'15.60"E). **c)** Bima Sandstone xenolith within the alkali basalt observed in Figure 4b. **d)** Plane-polarized (left) and cross-polarized (right) light photomicrographs of the alkali basalt observed in Figure 4b. Phenocrysts of clinopyroxene (Cpx) and olivine (Ol) are labelled. See text for details. Other volcanic cones with an alkali basalt composition occur at: (1) Lat. 10°15'57.88"N, Long. 11°27'41.28"E; and (2) Lat. 9°45'26.23"N, Long. 11° 7'50.58"E.

Figure 12. Schematic cross-section detailing possible mechanics of en-echelon formation.

Figure 13. Chronology of tectonic evolution, seafloor spreading, sedimentation, magmatism, and azimuthal changes in the Kane Fracture Zone related to the evolution of South Atlantic break-up. Igneous activity highlighted as follows: (1) Karroo and Patagonia; (2) Parana-Etendeka (P-E); (3) early P-E dykes; (4) primary phase of P-E bimodal volcanism; (5) late P-E dykes; (6) P-E alkaline magmatism; (7) widespread duration of alkaline magmatism (onshore, near-shore and oceanic); (8) igneous activity in Benue Trough recorded by dyke intrusion; (9) dyke intrusion in Benue Trough and

Brazil; (10) sub-alkaline, mafic magmatism in the Benue Trough, Campos, St Helena, and Rio Grande Rise; (11) pulse of alkaline/peralkaline magmatism; (12) oceanic and hotspot magmatism; and (13) Cenozoic igneous activity in Bornu Basin and other NE parts of Nigeria (Grant et al., 1972a). Timings of igneous activity in the Bornu Basin identified here (i.e. 1, 2, and 3) are compared to azimuthal changes in the Kane Fracture Zone and occurrence of major intra-continental unconformities across South America and Africa (yellow stars). Error bars for our proposed timings of igneous activity are shown and reflect uncertainties in the relative dating of events. Figure adapted from Torsvik et al., (2009) and Fairhead et al., (2013).

References

Alalade, B., and Tyson, R. V., 2013, Influence of igneous intrusions on thermal maturity of Late Cretaceous shales in the Tuma well, Chad Basin, NE Nigeria: Journal of African Earth Sciences, v. 77, p. 59-66.

Avbovbo, A., Ayoola, E., and Osahon, G., 1986, Depositional and structural styles in Chad Basin of northeastern Nigeria: Am. Assoc. Pet. Geol., Bull.;(United States), v. 70, no. 12.

Benkhelil, J., Dainelli, P., Ponsard, J., Popoff, M., and Saugy, L., 1988, The Benue Trough: Wrench fault related basin, on the border of the Equatorial Atlantic, Triassic-Jurassic Rifting—Continental Breakup and the Origin of the Atlantic Ocean and Passive Margins, Volume 22, Elsevier Amsterdam, p. 789-819.

Benkhelil, J., 1989, The origin and evolution of the Cretaceous Benue Trough (Nigeria): Journal of African Earth Sciences (and the Middle East), v. 8, no. 2, p. 251-282.

Berndt, C., Bünz, S., Clayton, T., Mienert, J., and Saunders, M., 2004, Seismic character of bottom simulating reflectors: examples from the mid-Norwegian margin: Marine and Petroleum Geology, v. 21, no. 6, p. 723-733.

Carter, J. D., W., B. A., Tait, E. A., and G.P., J., 1963, The geology of parts of Adamawa, Bauchi and Borno provinces in North - eastern Nigeria: Bullaten Geological Survey of Nigeria, v. 30, p. 1-108.

Cukur, D., Horozal, S., Kim, D. C., Lee, G. H., Han, H. C., and Kang, M. H., 2010, The distribution and characteristics of the igneous complexes in the northern East China Sea Shelf Basin and their implications for hydrocarbon potential: Marine Geophysical Researches, v. 31, no. 4, p. 299-313.

Davison, I. A. N., 1997, Wide and narrow margins of the Brazilian South Atlantic: Journal of the Geological Society, v. 154, no. 3, p. 471-476.

Dixon, R. J., Schofield, K., Anderton, R., Reynolds, A. D., Alexander, R. W. S., Williams, M. C., and Davies, K. G., 1995, Sandstone diapirism and clastic intrusion in the Tertiary submarine fans of the Bruce-Beryl Embayment, Quadrant 9, UKCS: Geological Society, London, Special Publications, v. 94, no. 1, p. 77-94.

Fairhead, J. D., 1988, Mesozoic plate tectonic reconstructions of the central South Atlantic Ocean: The role of the West and Central African rift system: Tectonophysics, v. 155, no. 1–4, p. 181-191.

Fairhead, J. D., Green, C. M., Masterton, S. M., and Guiraud, R., 2013, The role that plate tectonics, inferred stress changes and stratigraphic unconformities have on the evolution of the West and Central African Rift System and the Atlantic continental margins: Tectonophysics, v. 594, no. 0, p. 118-127.

Galerne, C. Y., Galland, O., Neumann, E.-R., and Planke, S., 2011, 3D relationships between sills and their feeders: evidence from the Golden Valley Sill Complex (Karoo Basin) and experimental modelling: Journal of Volcanology and Geothermal Research, v. 202, no. 3–4, p. 189-199.

Genik, G. J., 1992, Regional framework, structural and petroleum aspects of rift basins in Niger, Chad and the Central African Republic (C.A.R.): Tectonophysics, v. 213, no. 1–2, p. 169-185.

Grant, N., Rex, D., and Freeth, S., 1972a, Potassium-argon ages and strontium isotope ratio measurements from volcanic rocks in northeastern Nigeria: Contributions to Mineralogy and Petrology, v. 35, no. 4, p. 277-292.

Grant, N. K., Rex, D. C., and Freeth, S. J., 1972b, Potassium-argon ages and strontium isotope ratio measurements from volcanic rocks in northeastern Nigeria: Contributions to Mineralogy and Petrology, v. 35, no. 4, p. 277-292.

Guiraud, M., 1990, Tectono-sedimentary framework of the early Cretaceous continental Bima formation (upper Benue Trough, NE Nigeria): Journal of African Earth Sciences (and the Middle East), v. 10, no. 1–2, p. 341-353.

Guiraud, R., and Maurin, J.-C., 1992, Early Cretaceous rifts of Western and Central Africa: an overview: Tectonophysics, v. 213, no. 1–2, p. 153-168.

Guiraud, R., and Bosworth, W., 1997, Senonian basin inversion and rejuvenation of rifting in Africa and Arabia: synthesis and implications to plate-scale tectonics: Tectonophysics, v. 282, no. 1–4, p. 39-82.

Hansen, D. M., and Cartwright, J., 2006a, Saucer-shaped sill with lobate morphology revealed by 3D seismic data: implications for resolving a shallow-level sill emplacement mechanism: Journal of the Geological Society, v. 163, no. 3, p. 509-523.

Hansen, D. M., and Cartwright, J., 2006b, The three-dimensional geometry and growth of forced folds above saucer-shaped igneous sills: Journal of Structural Geology, v. 28, no. 8, p. 1520-1535.

Huuse, M., and Mickelson, M., 2004, Eocene sandstone intrusions in the Tampen Spur area (Norwegian North Sea Quad 34) imaged by 3D seismic data: Marine and Petroleum Geology, v. 21, no. 2, p. 141-155.

Jackson, C. A.-L., Schofield, N., and Golenkov, B., 2013, Geometry and controls on the development of igneous sill–related forced folds: A 2-D seismic reflection case study from offshore southern Australia: Geological Society of America Bulletin, v. 125, no. 11-12, p. 1874-1890.

Magee, C., Briggs, F., and Jackson, C. A.-L., 2013a, Lithological controls on igneous intrusion-induced ground deformation: Journal of the Geological Society, v. 170, no. 6, p. 853-856.

Magee, C., Hunt-Stewart, E., and Jackson, C. A. L., 2013b, Volcano growth mechanisms and the role of sub-volcanic intrusions: Insights from 2D seismic reflection data: Earth and Planetary Science Letters, v. 373, no. 0, p. 41-53.

Magee, C., Jackson, C. A.-L., and Schofield, N., 2013c, The influence of normal fault geometry on igneous sill emplacement and morphology: Geology, v. 41, no. 4, p. 407-410.

Magee, C., Jackson, C. A. L., and Schofield, N., 2014, Diachronous sub-volcanic intrusion along deep-water margins: insights from the Irish Rockall Basin: Basin Research, v. 26, no. 1, p. 85-105.

Magee, C., Maharaj, S. M., Wrona, T., and Jackson, C. A.-L., 2015, Controls on the expression of igneous intrusions in seismic reflection data: Geosphere, v. 11, no. 4, p. 1024-1041.

Magee, C., Muirhead, J. D., Karvelas, A., Jackson, C. A-L., Bastow, I., Holford, S. P., Schofield, N., Stevenson, C. T. E., McLean, C., McCarthy, W., and Shtukert, O., 2016, Lateral magma flow in sill-complexes: Geosphere, v. 12, no. 3, p. 1-33.

Malthe-Sørenssen, A., Planke, S., Svensen, H., and Jamtveit, B., 2004, Formation of saucer-shaped sills: Geological Society, London, Special Publications, v. 234, no. 1, p. 215-227.

Meeuws, F. J. E., Holford, S. P., Foden, J. D., and Schofield, N., 2016, Distribution, chronology and causes of Cretaceous – Cenozoic magmatism along the magma-poor rifted southern Australian margin: Links between mantle melting and basin formation: Marine and Petroleum Geology, v. 73, p. 271-298.

Nelson, C. E., Jerram, D. A., and Hobbs, R. W., 2009, Flood basalt facies from borehole data: implications for prospectivity and volcanology in volcanic rifted margins: Petroleum Geoscience, v. 15, no. 4, p. 313-324.

Obaje, N. G., Wehner, H., Abubakar, M. B., and Isah, M. T., 2004a, Nasara-I Well, Gongola Basin (Upper Benue Trough, Nigeria): Source-Rock Evaluation: Journal of Petroleum Geology, v. 27, no. 2, p. 191-206.

Obaje, N. G., Wehner, H., Hamza, H., and Scheeder, G., 2004b, New geochemical data from the Nigerian sector of the Chad basin: implications on hydrocarbon prospectivity: Journal of African Earth Sciences, v. 38, no. 5, p. 477-487.

Pérez-Díaz, L., and Eagles, G., 2014, Constraining South Atlantic growth with seafloor spreading data: Tectonics, v. 33, no. 9, p. 1848-1873.

Planke, S., Symonds, P. A., Alvestad, E., and Skogseid, J., 2000, Seismic volcanostratigraphy of large-volume basaltic extrusive complexes on rifted margins: Journal of Geophysical Research, v. 105, no. B8, p. 19335-19351.

Planke, S., Rasmussen, T., Rey, S. S., And Myklebust, R., 2005, Seismic characteristics and distribution of volcanic intrusions and hydrothermal vent complexes in the Vøring and Møre basins: Geological Society, London, Petroleum Geology Conference series, v. 6, p. 833-844.

Planke, S., Svensen, H., Myklebust, R., Bannister, S., Manton, B., and Lorenz, L., 2015, Geophysics and Remote Sensing: Berlin, Heidelberg, Springer Berlin Heidelberg, p. 1-16.

Pollard, D. D., Muller, O. H., and Dockstader, D. R., 1975, The form and growth of fingered sheet intrusions: Geological Society of America Bulletin, v. 86, no. 3, p. 351-363.

Polteau, S., Mazzini, A., Galland, O., Planke, S., and Malthe-Sørenssen, A., 2008, Saucer-shaped intrusions: Occurrences, emplacement and implications: Earth and Planetary Science Letters, v. 266, no. 1–2, p. 195-204.

Rickwood, P., 1990, The anatomy of a dyke and the determination of propagation and magma flow directions: Mafic dykes and emplacement mechanisms, p. 81-100.
Samaila, N., Abubakar, M., Dike, E., and Obaje, N., 2006, Description of soft-sediment deformation structures in the Cretaceous Bima Sandstone from the Yola Arm, Upper Benue Trough, Northeastern Nigeria: Journal of African Earth Sciences, v. 44, no. 1, p. 66-74.
Schofield, N., Stevenson, C., and Reston, T., 2010, Magma fingers and host rock fluidization in the emplacement of sills: Geology, v. 38, no. 1, p. 63-66.
Schofield, N., Heaton, L., Holford, S. P., Archer, S. G., Jackson, C. A.-L., and Jolley, D. W., 2012a, Seismic imaging of 'broken bridges': linking seismic to outcrop-scale investigations of intrusive magma lobes: Journal of the Geological Society, v. 169, no. 4, p. 421-426.
Schofield, N. J., Brown, D. J., Magee, C., and Stevenson, C. T., 2012b, Sill morphology and comparison of brittle and non-brittle emplacement mechanisms: Journal of the Geological Society, v. 169, no. 2, p. 127-141.
Schofield, N., Holford, S., Millett, J., Brown, D., Jolley, D., R. Passey, S., Muirhead, D., Grove, C., Magee, C., Murray, J., Hole, M., A.-L. Jackson, C., and Stevenson, C., 2015, Regional magma plumbing and emplacement mechanisms of the Faroe-Shetland Sill Complex: implications for magma transport and petroleum systems within sedimentary basins: Basin Research, p. n/a-n/a.
Sengör, A. M. C., and Burke, K., 1978, Relative timing of rifting and volcanism on Earth and its tectonic implications: Geophysical Research Letters, v. 5, no. 6, p. 419-421.
Skogseid, J., Pedersen, T., Eldholm, O., and Larsen, B. T., 1992, Tectonism and magmatism during NE Atlantic continental break-up: the Vøring Margin: Geological Society, London, Special Publications, v. 68, no. 1, p. 305-320.
Smallwood, J. R., and Maresh, J., 2002, The properties, morphology and distribution of igneous sills: modelling, borehole data and 3D seismic from the Faroe-Shetland area: Geological Society, London, Special Publications, v. 197, no. 1, p. 271-306.
Symonds, P., Planke, S., Frey, O., and Skogseid, J., 1998, Volcanic evolution of the Western Australian continental margin and its implications for basin development: The sedimentary basins of Western Australia, v. 2, p. 33-54.
Thomson, K., and Hutton, D., 2004, Geometry and growth of sill complexes: insights using 3D seismic from the North Rockall Trough: Bulletin of Volcanology, v. 66, no. 4, p. 364-375.
Thomson, K., 2007, Determining magma flow in sills, dykes and laccoliths and their implications for sill emplacement mechanisms: Bulletin of Volcanology, v. 70, no. 2, p. 183-201.
Torsvik, T. H., Rousse, S., Labails, C., and Smethurst, M. A., 2009, A new scheme for the opening of the South Atlantic Ocean and the dissection of an Aptian salt basin: Geophysical Journal International, v. 177, no. 3, p. 1315-1333.
Trude, J., Cartwright, J., Davies, R. J., and Smallwood, J., 2003, New technique for dating igneous sills: Geology, v. 31, no. 9, p. 813-816.
Valentine, G. A., and Perry, F. V., 2007, Tectonically controlled, time-predictable basaltic volcanism from a lithospheric mantle source (central Basin and Range Province, USA): Earth and Planetary Science Letters, v. 261, no. 1–2, p. 201-216.

Vigneresse, J. L., and Clemens, J. D., 2000, Granitic magma ascent and emplacement: neither diapirism nor neutral buoyancy: Geological Society, London, Special Publications, v. 174, no. 1, p. 1-19.

White, R., and McKenzie, D., 1989, Magmatism at rift zones: The generation of volcanic continental margins and flood basalts: Journal of Geophysical Research: Solid Earth, v. 94, no. B6, p. 7685-7729.

Xu, Y., Huang, W., Chen, T., Cui, R., and Chen, S., 2009, An evaluation of deep thin coal seams and water-bearing/resisting layers in the quaternary system using seismic inversion: Mining Science and Technology (China), v. 19, no. 2, p. 161-165.

Xu, Y., Chen, T., Chen, S., Huang, W., and Wu, G., 2010, Comparison between several seismic inversion methods and their application in mountainous coal fields of western China: Mining Science and Technology (China), v. 20, no. 4, p. 585-590.

Zampetti, V., Sattler, U., and Braaksma, H., 2005, Well log and seismic character of Liuhua 11-1 Field, South China Sea; relationship between diagenesis and seismic reflections: Sedimentary Geology, v. 175, no. 1–4, p. 217-236.

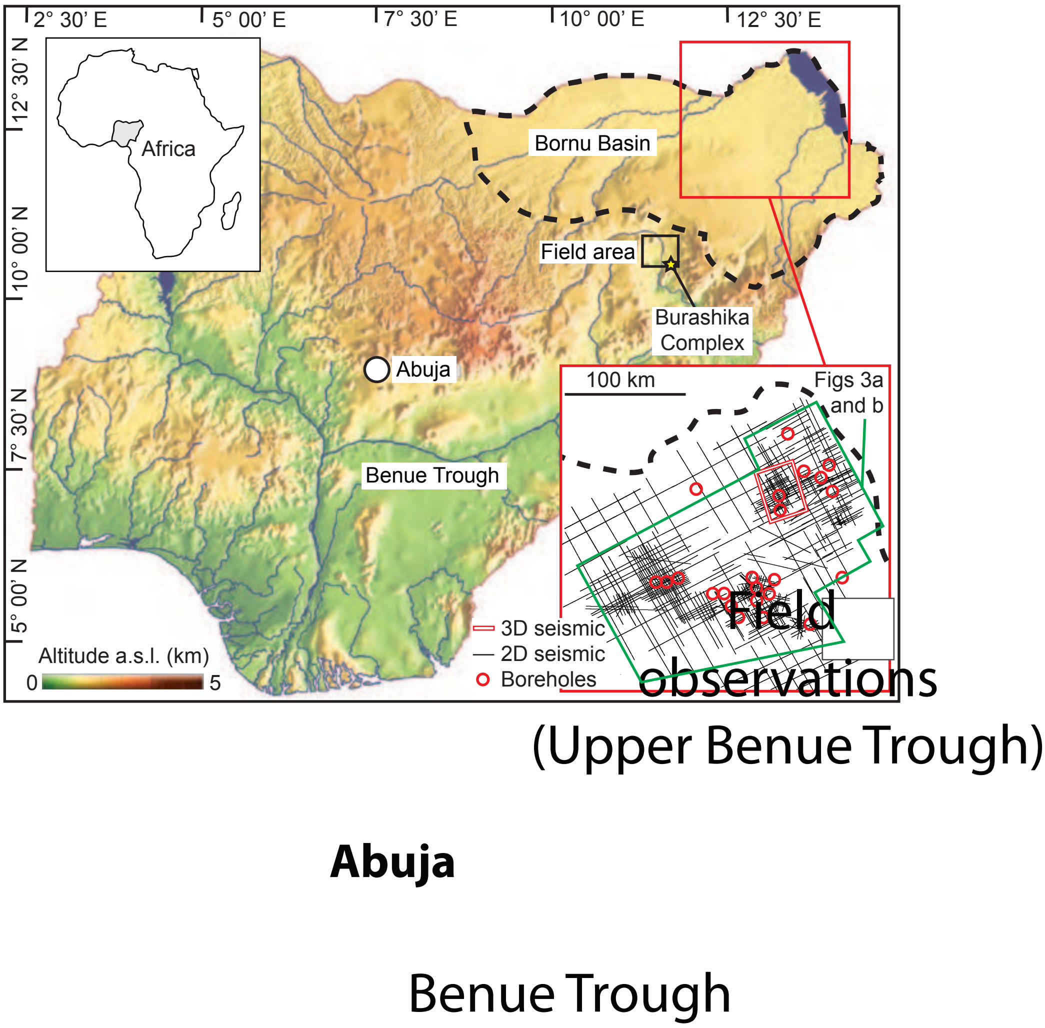
2° 30' E
5° 00' E
7° 30' E
10° 00' E
12° 30' E
12° 30' N
10° 00' N
7° 30' N
5° 00' N
Africa
Bornu Basin
Field area
Burashika Complex
Abuja
Benue Trough
100 km
Figs 3a and b
3D seismic
2D seismic
Boreholes
Altitude a.s.l. (km)
0
5
Field observations
(Upper Benue Trough)
Abuja
Benue Trough

Figure 2

Click here to download Figure Fig. 2 - strat column.pdf

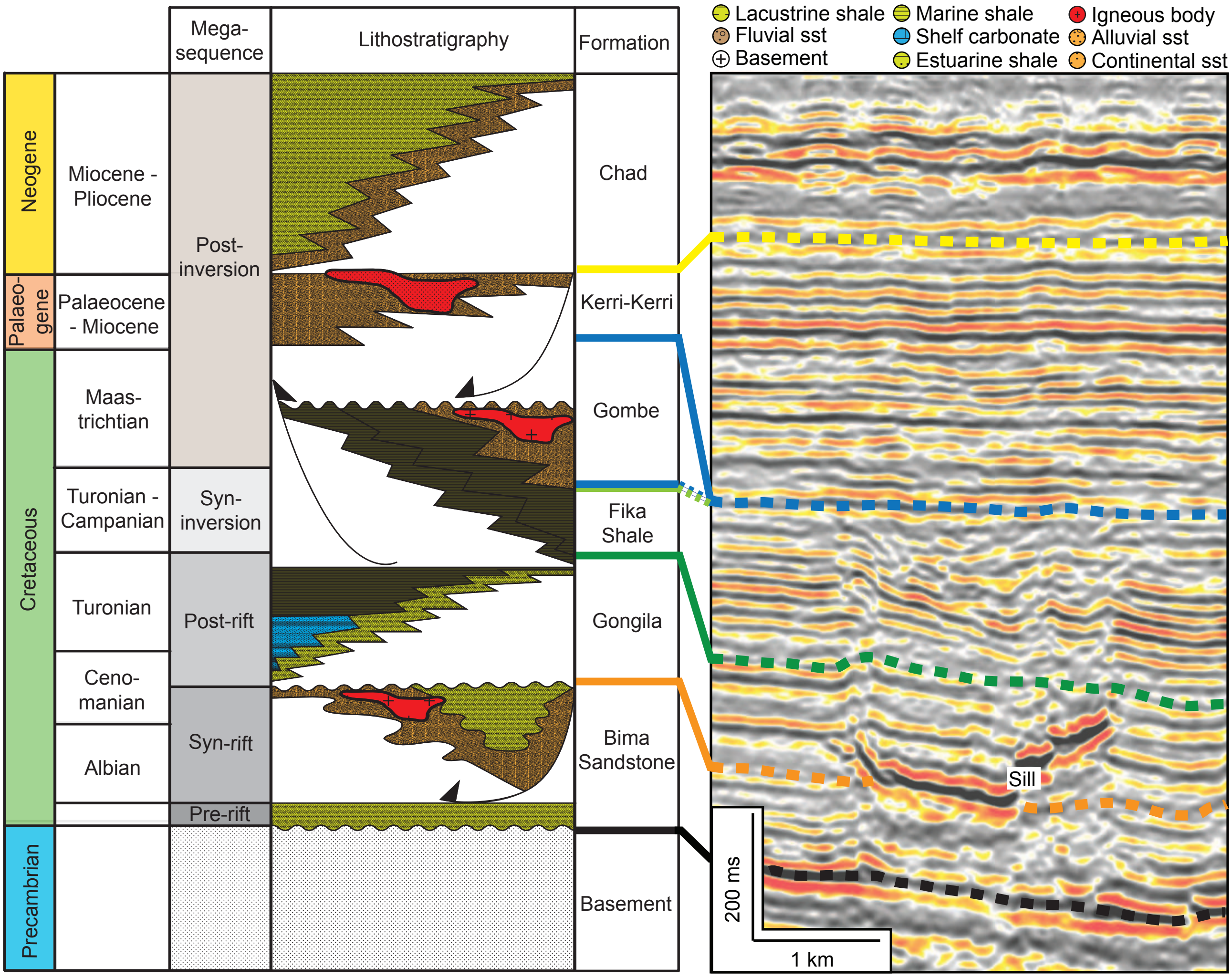

Figure 3

Click here to download Figure Fig. 3 - maps.pdf

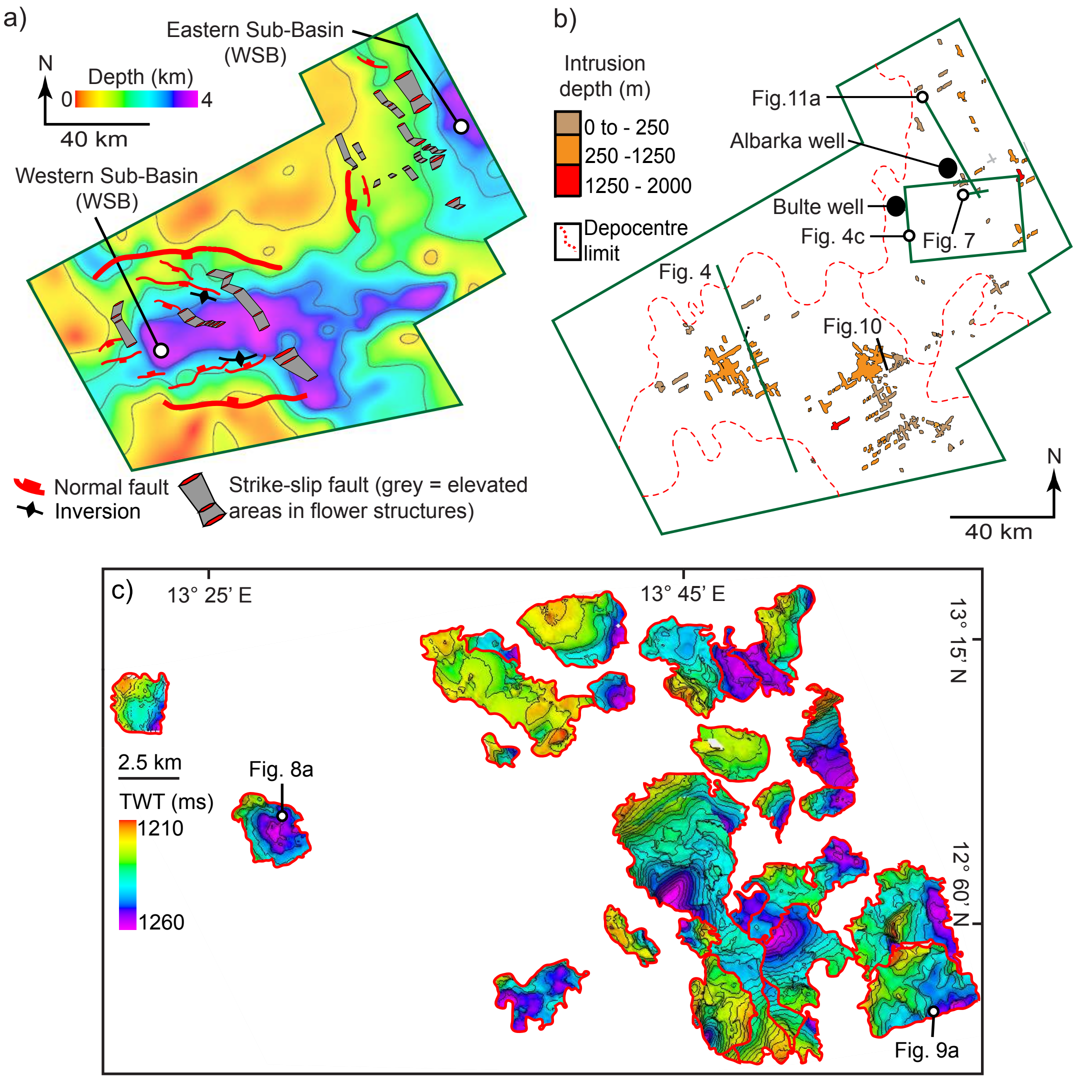

Figure 4

Click here to download Figure Fig. 4 - regional seismic.pdf

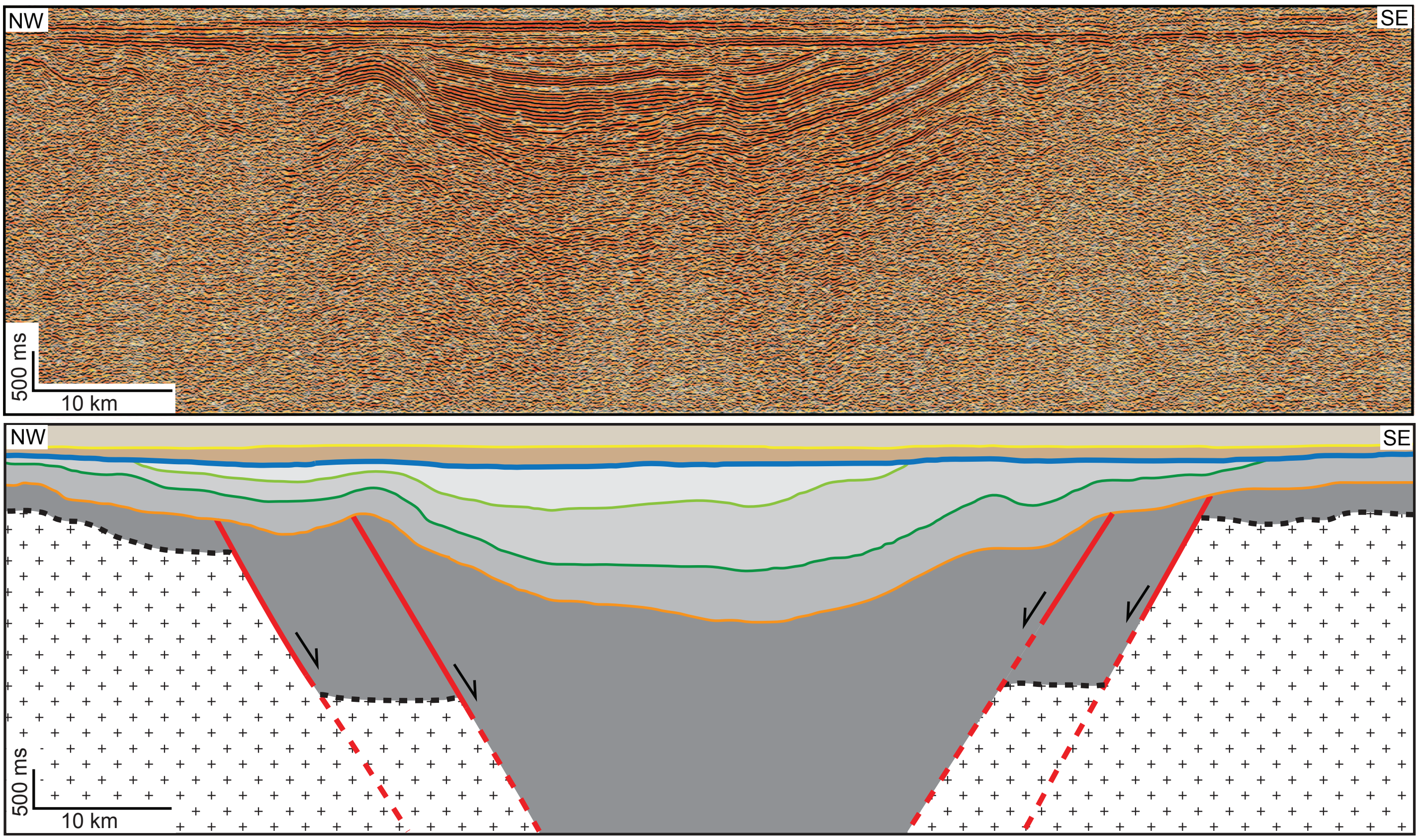

Figure 5

Click here to download Figure Fig. 5 - magma flow indicators.pdf

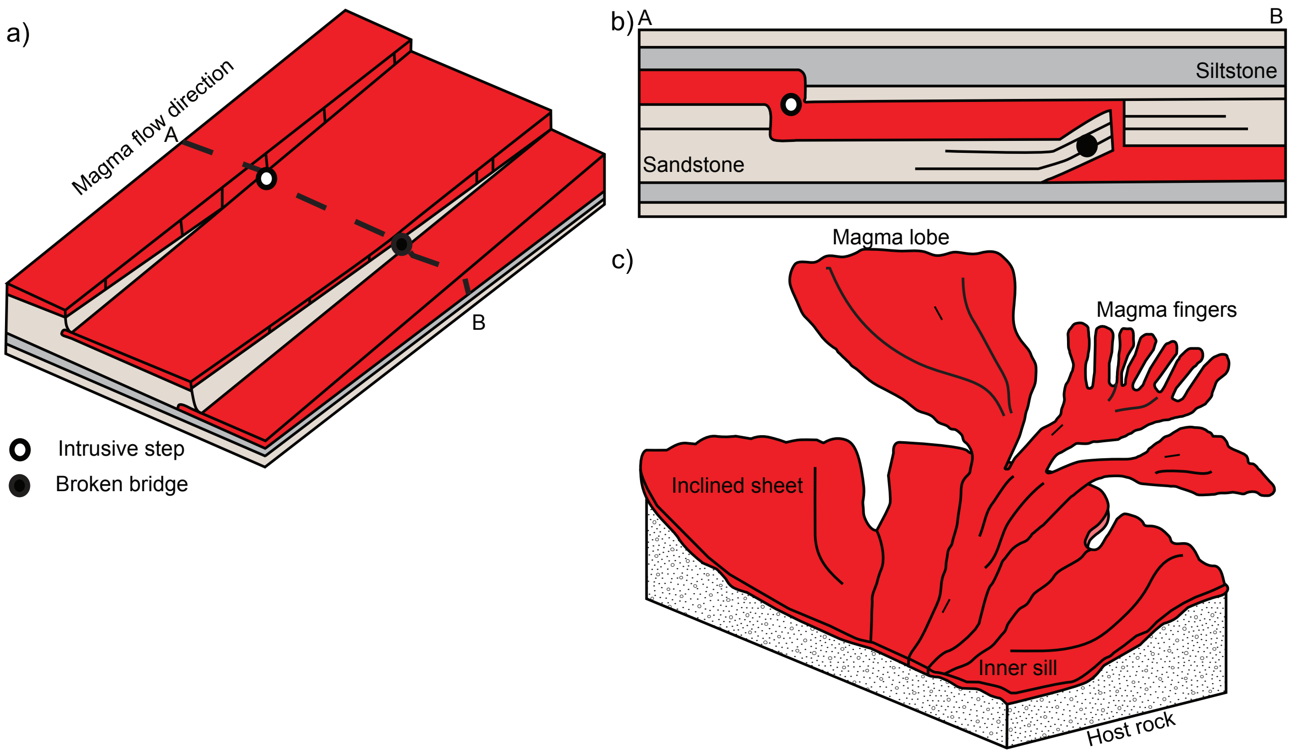

Figure 6

Click here to download Figure Fig. 6 - well correlation.pdf

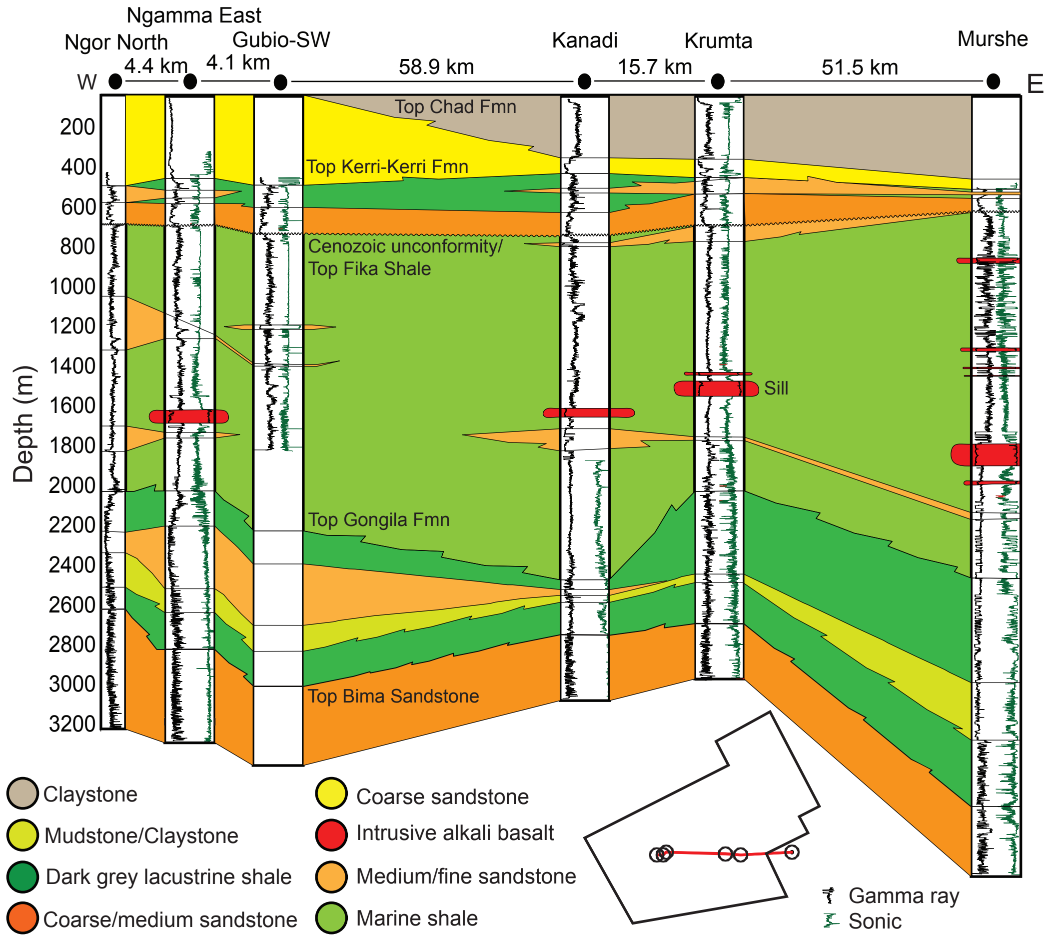

Figure 7

Click here to download Figure Fig. 7 - sill uc relationship.pdf

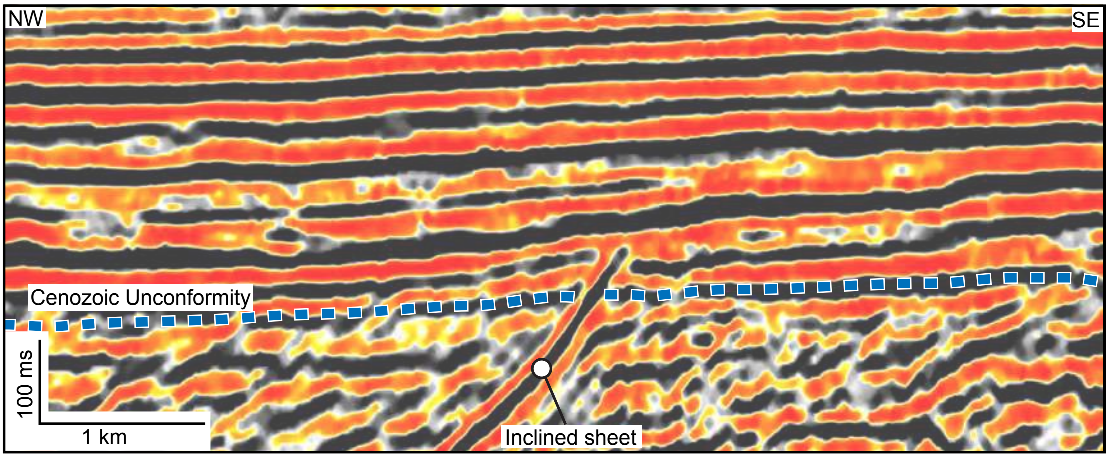

Figure 8

Click here to download Figure Fig. 8 - sill and flower structure.pdf

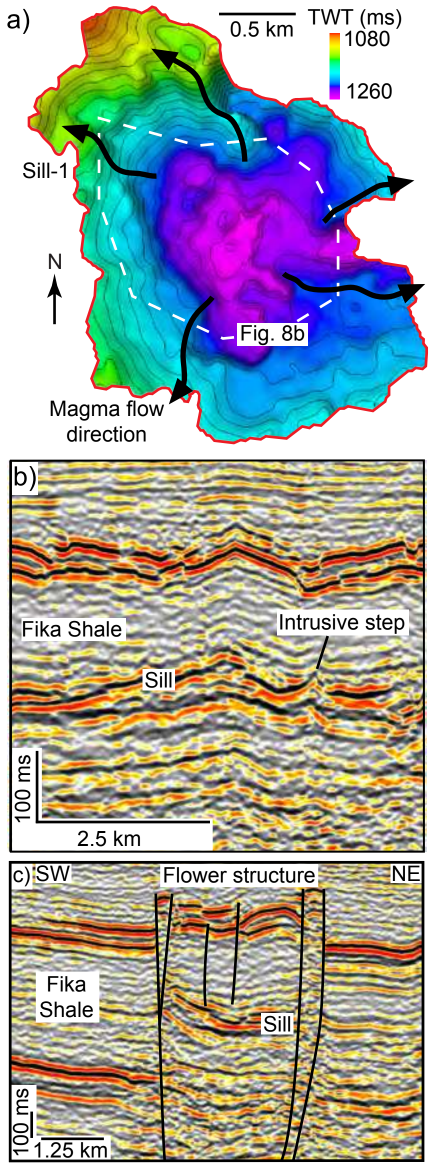

Figure 9

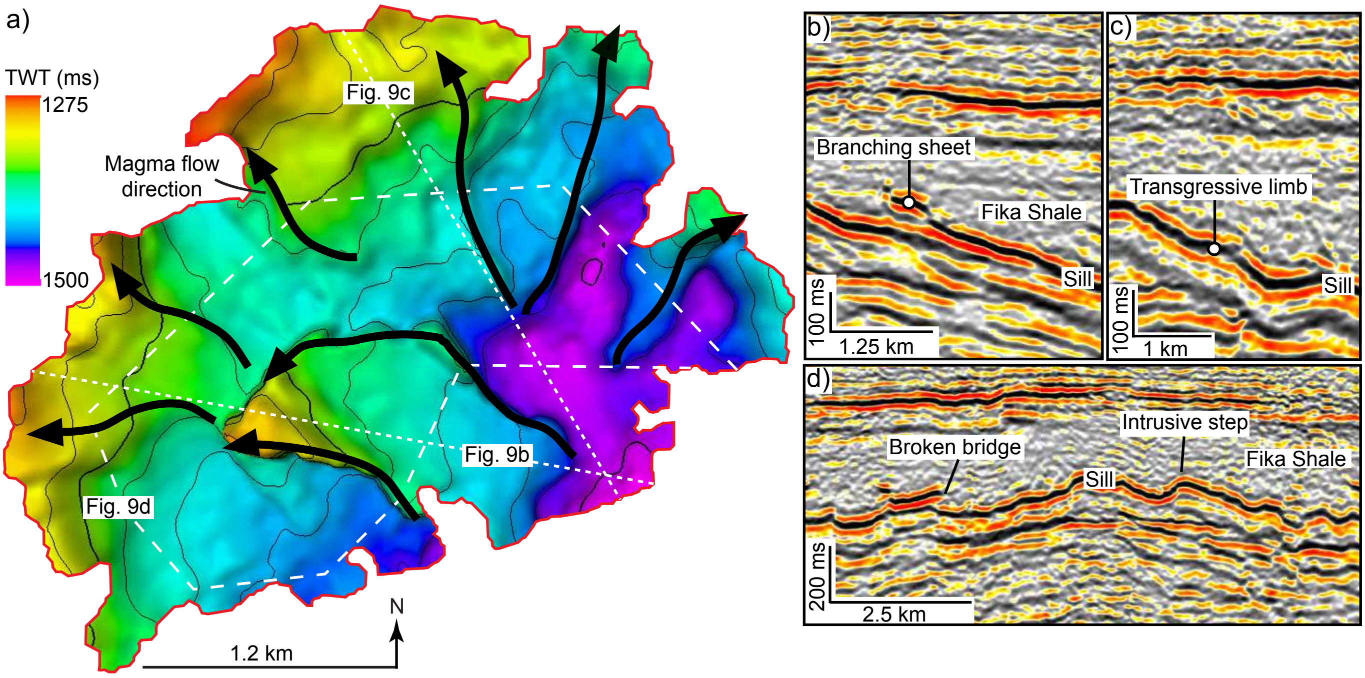
a)
TWT (ms)
1275
1500
Magma flow direction
Fig. 9c
Fig. 9b
Fig. 9d
1.2 km
N
b)
Branching sheet
Fika Shale
Sill
100 ms
1.25 km
c)
Transgressive limb
Sill
100 ms
1 km
d)
Broken bridge
Intrusive step
Fika Shale
Sill
200 ms
2.5 km

Figure 10

Click here to download Figure Fig. 10 - forced fold.pdf

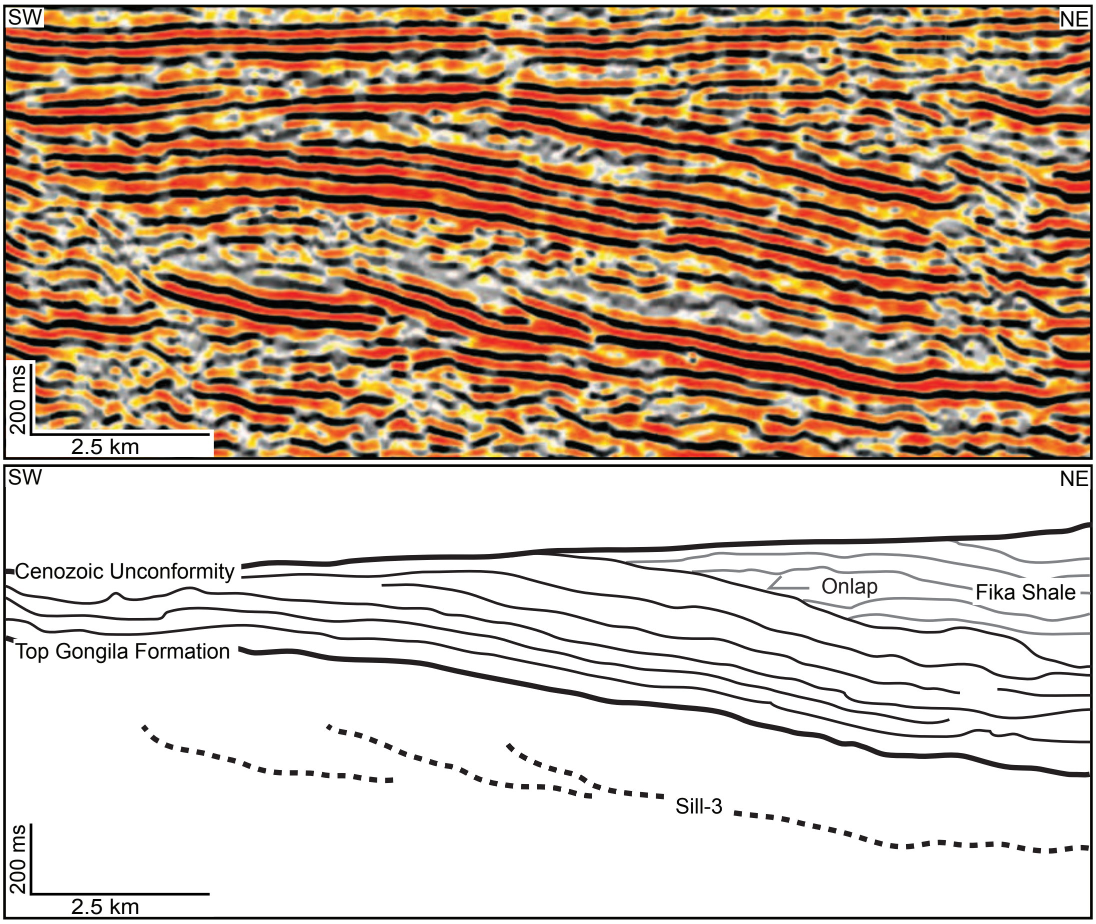

Figure 11

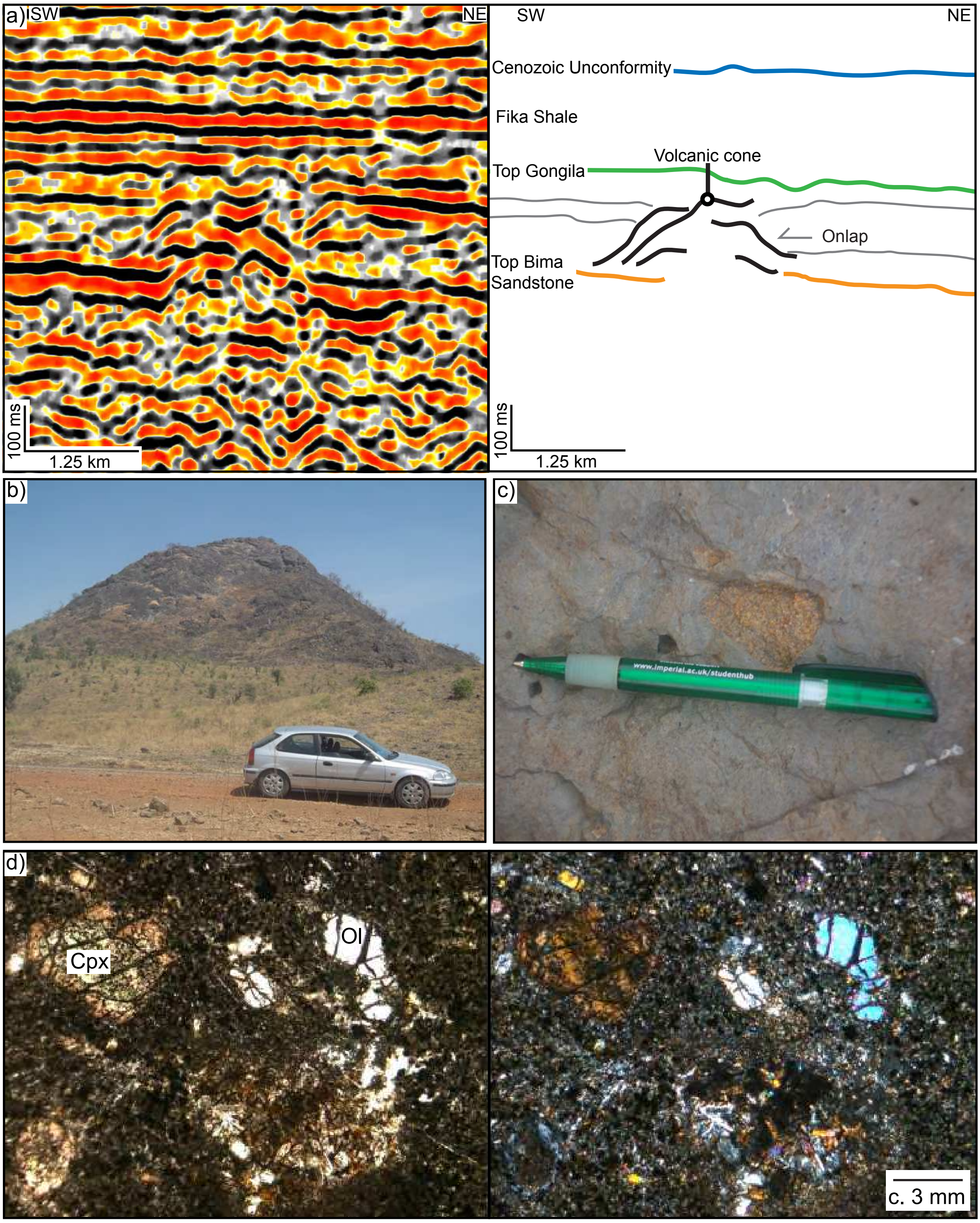
a)
SW
NE
100 ms
1.25 km
SW
NE
Cenozoic Unconformity
Fika Shale
Volcanic cone
Top Gongila
Onlap
Top Bima
Sandstone
100 ms
1.25 km
b)
c)
www.imperial.ac.uk/studenthub
d)
Cpx
Ol
c. 3 mm

Figure 12

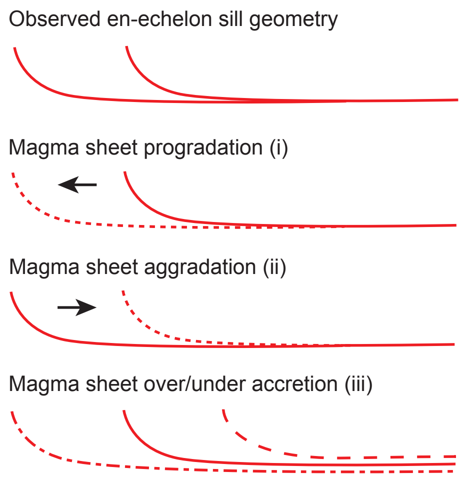
Observed en-echelon sill geometry
Magma sheet progradation (i)
Magma sheet aggradation (ii)
Magma sheet over/under accretion (iii)

Figure 13 Click here to download Figure Fig. 13 - summary timing.pdf